Contents lists available at ScienceDirect

International Journal of Non-Linear Mechanics

journal homepage: www.elsevier.com/locate/nlm

Highlights

Dynamics of accelerating and decelerating flows: A boundary layer examination with non-similar approach and convective boundary condition

International Journal of Non-Linear Mechanics xxx (xxxx) xxx

Mojeed T. Akolade, Gabriel Samaila*, Micheal Oni, Abdulhakeem Yusuf, Peter Bukar Malgwi, Taiwo S. Yusuf, Yusuf O. Tijani

- Boundary layer over an inclined plate.
- Non-similar solution for natural convection flow.
- Effect of thermal radiation on boundary layer flow.
- Casson fluid flow over an inclined plate.

Contents lists available at ScienceDirect

International Journal of Non-Linear Mechanics

journal homepage: www.elsevier.com/locate/nlm

Dynamics of accelerating and decelerating flows: A boundary layer examination with non-similar approach and convective boundary condition☆

Mojeed T. Akolade [a,b], Gabriel Samaila [c,*], Micheal Oni [d], Abdulhakeem Yusuf [e], Peter Bukar Malgwi [c], Taiwo S. Yusuf [d], Yusuf O. Tijani [f]

[a] Department of Computer Science, Lead City University, Ibadan, Nigeria
[b] Department of Mathematics, University of Ilorin, Ilorin, Nigeria
[c] Department of Mathematics, Air Force Institute of Technology, Kaduna, Nigeria
[d] Department of Mathematics, Ahmadu Bello University, Zaria, Nigeria
[e] Department of Mathematics, Federal University of Technology, Minna, Nigeria
[f] Department of Mathematics, Rhodes University, Makhanda, P.O Box 94, Grahamstown 6140, South Africa

ARTICLE INFO

Keywords:
Casson
Stretching/shrinking sheet
Non-similar solution
Dufour/Soret effect
Nanoparticle
MHD

ABSTRACT

Moisture/air-flow over the aircraft wing and bonnet of a moving car in aerodynamical systems exhibit dynamic behavior characterized by accelerating and decelerating flows. These analysis is essential and applicable in various fields, including physics, engineering, and fluid mechanics. The present investigation aim to explore the dynamics of accelerating and decelerating flows within the framework of boundary layer examination. To achieve these objectives, a non-similar group of transformations is employed to convert the governing dimensional two-variable dynamical system into a dimensionless differential form, with η and ξ as the independent variables. To gain physical understanding of the mathematical equations governing the flow, an efficient bivariate spectral collocation method (BSCM) is employed for analyzing the flow dynamics. This method allows for a thorough investigation of the behavior and characteristics of the accelerating and decelerating Casson flows. Subject to the convergence and residual error analysis of the numerical results, the effects of pertinent parameters on the flow variables were investigated. The findings of this study show that the effects of flow parameters on decelerating and accelerating flows are not completely opposite. Additionally, the Biot parameter positively impacts the velocity and temperature profiles of the two dynamical flows. However, an increase in the Casson fluid parameter β has an opposing effect on the temperature and concentration profiles of both flows.

1. Introduction

The study of accelerating or decelerating flow around a surface holds significant applications in the stability analysis of aircraft, determination of aircraft speed, and enhancement in the design of high-speed trains, vehicles, or aircraft. Sundstrom and Cervantes [1] investigated the similarities between accelerating and decelerating flows. The study revealed that the time developments of mean and turbulent properties in accelerating and decelerating flows exhibit similarity during an initial phase after the transient period. In another work [2], they explored the self-similarity of wall-bounded temporally accelerating turbulent flows, while Seddighi et al. [3] employed a direct numerical solution to study accelerating fluid around a tube. Additionally, Guerrero et al. [4] discussed the behavior of decelerating flow at a transient state. Other important literature discussing the applications of accelerating and decelerating flows includes Refs. [5–7].

Obtaining analytical and approximation solutions for non-Newtonian fluids is challenging due to the complexity inherent in their nonlinear structure, a difficulty that is particularly to the Casson fluid model. According to Sparrow et al. [8], a non-similar boundary layer can arise due to various influences such as alterations in wall temperature, surface mass transfer, free stream velocity, the introduction of fluid through injection/suction on the surface, the impact of buoyancy forces, the influence of inclination angles, and other factors. To predict the ideal solution for dynamical flows intended for engineering and scientific applications, conventional similar solution techniques prove inadequate as they do not sufficiently account for all independent

☆ Computational Mechanics and Mathematical Modelling Research Group (CMMMRG).

* Corresponding author.
E-mail addresses: akolade.mojeed@lcu.edu.ng (M.T. Akolade), gabbbooooo@yahoo.com (G. Samaila), michaeloni29@yahoo.com (M. Oni), yusuf.abdulhakeem@futminna.edu.ng (A. Yusuf), bumalpeter@gmail.com (P.B. Malgwi), taiyeee@yahoo.com (T.S. Yusuf), yusuf.tijani@ru.ac.za (Y.O. Tijani).

https://doi.org/10.1016/j.ijnonlinmec.2024.104675
Received 20 November 2023; Received in revised form 17 January 2024; Accepted 12 February 2024

Nomenclature

$Le = \frac{\nu}{D_B}$	Lewis number
$Sr = \frac{D_T}{D_f}\frac{D_T}{D_B}\frac{k_T}{T_\infty}$	Soret number
$N_t = \frac{T D_T \Delta T}{T_\infty \nu}$	Thermophoretic parameter
$N_b = \frac{T D_B \Delta C}{\nu}$	Brownian motion parameter
$Pr = \frac{\nu \rho C_p}{k_f}$	Prandtl number
$N_r = \frac{4\sigma T^{*3}_\infty}{k_f k^*}$	Thermal radiation parameter
$D_u = \frac{D_T K_T}{C_s C_p}\frac{\Delta C}{\Delta T}\frac{\rho C_p}{k_f}$	Dufour parameter
$Ha^2 = \frac{\sigma B_0^2}{\rho_f \lambda b}$	Magnetic number
$G_c = \frac{\beta_c \Delta C}{\beta_t \Delta T}$	Solutal Grashof number
$G_r = \frac{g\beta_t \Delta T L}{\lambda^2 b^2}$	Thermal Grashof number
$Bi = \frac{h_f}{\kappa_f} L^{\frac{1-Z}{2}} \left(\frac{\nu}{\lambda b}\right)^{1/2}$	Biot number
β	Casson parameter

variables [9,10]. While several self-group theories have been adopted to address this challenge [2,11–14], Lawal and Ajadi [15] provided local non-similarity solutions for the flow of Casson. These approaches are specific to particular problems. To circumvent doubts in the solutions arising from self-similarity results, truncation errors in perturbation series, and to avoid the occurrence of intersection and violation of boundary conditions commonly referred to as "common errors made in the investigation of boundary layer flows", dimensional problems are transformed and solved using a non-similar approach. Through this method, the coordinates x and y are eliminated by an appropriate transformation in the modified equations of a dimensional partial differential equation (PDE) problem, resulting in dimensionless systems with coordinates η and ξ (White [16]).

Numerous investigations into this analysis include the recent non-similar solution of Casson fluid boundary layer flow by Bisht and Sharma [17], the utilization of the non-similar approach for solving the conjugate gradient problem by Khademi et al. [18], and Kaya [19]). Yih [20], in his study on non-Darcy MHD natural convection flow encompassing viscous and Joule heating effects over a permeable sphere, considered this approach. The dynamics of Reiner-Philippoff (RP) fluid by Tijani et al. [21–23] justify the accuracy and efficiency of the non-similar technique in solving engineering and biological systems. Other notables studies can found in the recent study of Mustafa et al. [24] for the solution power-law fluid flow over a moving wedge, Cui et al. [25] on the forced convection analysis of nano-fluid flow over stretching surface, Farooq et al. [26], to mention few.

In the context of heat and mass transfer within a moving fluid flow, Soret-Dufour factor plays a pivotal role, being indispensable for tasks like shaping nuclear reactor designs, harnessing geothermal energy, managing the movement of groundwater pollutants, overseeing oil reservoir dynamics, enabling isotope separation, manufacturing rubber and plastic sheets, blending gas compositions, optimizing compact heat insulation exchangers, and facilitating the responsible disposal of nuclear waste, alongside various other practical applications. Gajjela and Garvandha [27] analyzed the characteristics of thermo-diffusion and diffusion-thermo effects mixed with chemical reaction of MHD pair stress liquid over an extended cylinder. A model encompassing the effects of thermal radiation, and slip on bio-convection of an Oldroyd-B nanoliquid was numerically investigated by Tlili and Waqas [28]. In their study, extra impact of convective heating and absence of mass flux improves the fluid flow. Shojaei et al. [29] presented a depiction of the radiative flux involving the Dufour and Soret effects in the context of a second-grade fluid flowing on an elongated cylinder. The study indicated that as the Schmidt and Prandtl numbers increase, the solutal and thermal fields converge. Also, Jawad and Saeed [30] investigated the impact of Dufour and Soret effects on Maxwell fluid on an elongated surface with permeability using the Buongiorno model. In general, the Soret and Dufour parameters increase mass transfer but decrease Nusselt number. Other physical situations where the Soret and Dufour effects have been extensively analyzed can be seen in Ref. [31–36].

In recent times, scientists and engineers are focusing on the behavior of non-Newtonian and Newtonian fluid flows on expanding and contracting surfaces, particularly in various industrial fields like polymer processing, glass fiber production, and others. The flow of Casson fluid is characterized by the dominance of its shear stress magnitude over a yielded shear stress. This fluid's fundamental basis is rooted in a structural representation of the interaction between solid and liquid components in a double-phase suspension. Examples of Casson fluids include jelly, honey, concentrated fruit juice, synthetic fiber, and soup. Various products, such as paints, pharmaceutical substances, synthetic lubricants, china clay, tomato sauce, and coal, leverage the characteristics of Casson fluid in their manufacturing processes. Human blood is also considered a Casson fluid due to its composition of red blood cells, globulin, fibrinogen, and proteins in an aqueous plasma medium [37–39].

Pioneering discussions on Casson fluid flow through tubes were initiated by Oka [40], while Bhattacharyya et al. [41] explored magnetohydrodynamic flow over contracting/expanding sheets, emphasizing the uniqueness of the similarity solution in the presence of a stronger magnetic field. Mernone et al. [42] investigated two-dimensional peristaltic channel flow of Casson fluid, and Mustapha et al. [43] studied heat transfer with a time-dependent Casson model in a boundary layer over a moving plate. Mukhopadhyay [44] examined the effects of thermal radiation and heat blowing/suction on Casson fluid flow over stretched sheets, while Pramanik [45] systematically investigated the impact of porosity and radiant heat flow on heat and mass transfer. Arthur et al. [46] considered the influence of magnetic fields and chemical reactions, and Anwar et al. [47] explored transient magnetohydrodynamic movement of Casson fluid on an unbounded vertical plate under varying temperature and velocity conditions. Singh et al. [48] discussed the boundary layer motion of a laminar conductive Casson fluid induced by a horizontal porous sheet undergoing linear contraction/expansion with mass transpiration. Additional literature on Casson fluid can be found in Refs. [49–51]. The motivation for experiments on shrinking/stretching sheets lies in addressing transportation challenges, making this model widely applicable in engineering and industrial operations such as metal thinning, sheet extrusion, and heat exchange. The stretching sheet problem, initially investigated by Sakiadis [52,53], was further elucidated by Aly and Pop [54] through the study of flow through a moving sheet.

The novelty of this work lies in presenting a non-similar approach to investigate the Soret, Dufour, and radiation effects on accelerating or decelerating flow around a surface. The non-similar method is justified based on the non-vanishing of coordinates x and y for some physical parameters while using a similar analysis. Such solutions warrant considerable attention as they provide valuable insights for optimizing the design of supersonic vehicles, trains, and aircraft.

2. Mathematical statement

Consider two-dimensional laminar boundary layer flow of Casson nanofluid over a non-linear radiated slanted extending surface with convective surface boundary condition. The free stream and extending velocity are considered to be $U_\infty(x) = 0$ and $U_w(x) = ax^z$. Where x represents the coordinate in the direction of the extended surface with a constant a. A transverse magnetic field is assumed normal to the flow path. The thermophoresis and Brownian motion effect is considered to be very significant due to the presence of the nanoparticle. The constants of the fluid temperature T and the nanoparticle fraction

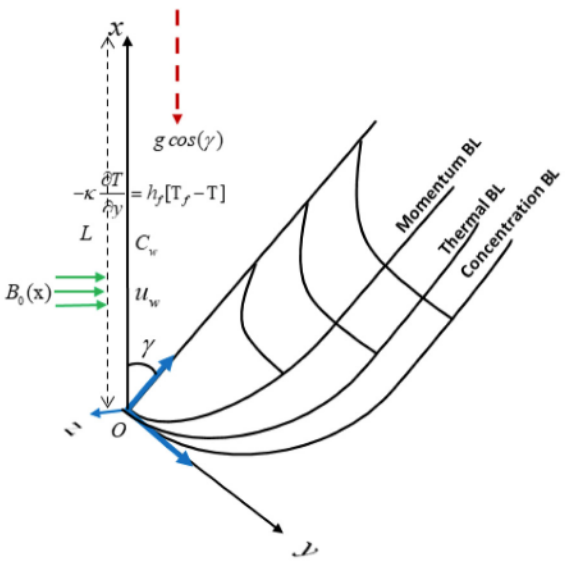

Fig. 1. Model physical coordinate geometry of boundary layer flow of Casson fluid.

C at the wall surface are considered to be T_w and C_w while the ambient nanofluid mass and temperature C_∞ and T_∞ are achieved as y approaches to immensity as demonstrated in Fig. 1 (see [8,15,34,55]).

Utilizing the Roseland approximation, the governing equation can be written as;

$$\frac{\partial u}{\partial x}+\frac{\partial v}{\partial y}=0, \tag{1}$$

$$u\frac{\partial u}{\partial x}+v\frac{\partial u}{\partial y}=\nu\left(1+\frac{1}{\beta}\right)\frac{\partial^2 u}{\partial y^2}+g\left[\beta_t(T-T_\infty)+\beta_c(C-C_\infty)\right]\cos\gamma-\frac{\sigma B^2(x)u}{\rho}, \tag{2}$$

$$u\frac{\partial T}{\partial x}+v\frac{\partial T}{\partial y}=\alpha\left[\frac{\partial^2 T}{\partial y^2}-\frac{1}{k}\frac{\partial q_r}{\partial y}\right]+\left[D_B\frac{\partial C}{\partial y}\frac{\partial T}{\partial y}+\frac{D_T}{T_\infty}\left(\frac{\partial T}{\partial y}\right)^2\right]+\frac{D_T K_T}{C_s C_p}\frac{\partial^2 C}{\partial y^2}, \tag{3}$$

$$u\frac{\partial C}{\partial x}+v\frac{\partial C}{\partial y}=D_B\frac{\partial^2 C}{\partial y^2}+\frac{D_T K_T}{T_\infty}\frac{\partial^2 T}{\partial y^2}, \tag{4}$$

The boundary conditions are defined as

$$\begin{aligned} &u=u_w,\quad v=0,\quad -k_f\frac{\partial T}{\partial y}=h_f\left(T_f-T\right),\quad C=C_w\quad at\quad y=0,\\ &u\to u_\infty(x),\quad T\to T_\infty,\quad C\to C_\infty\quad at\quad y\to\infty, \end{aligned} \tag{5}$$

where $U_w=\lambda b x^Z$, $B(x)=B_0 x^{\frac{Z-1}{2}}$, $U_\infty=\lambda a x^Z$.

2.1. Solution through the non-similar transformation

We define the following variables (see [8,15,34,55]);

$$u=\frac{\partial\psi}{\partial y},\qquad v=-\frac{\partial\psi}{\partial x},\qquad \psi=(\lambda\nu b)^{1/2}x^{\frac{Z+1}{2}}f(\xi,\eta), \tag{6}$$

$$\eta=y\left(\frac{\lambda b}{\nu}\right)^{1/2}x^{\frac{Z-1}{2}},\qquad \xi=\frac{x}{L},\qquad T=\Delta T\theta+T_\infty,\qquad C=\Delta C\phi+C_\infty, \tag{7}$$

$$\begin{aligned} &u=\nu b x^Z f'(\xi,\eta),\\ &v=-(\lambda\nu b)^{1/2}x^{\frac{Z-1}{2}}\left(\frac{Z+1}{2}\right)f-\lambda b y x^{Z-1}(Z-1)f'-(\lambda\nu b)^{1/2}x^{\frac{Z+1}{2}}\frac{\partial f}{\partial\xi}, \end{aligned} \tag{8}$$

Utilizing Eqs. (6)–(8) in to Eqs. (1)–(3) yield

$$\left(1+\frac{1}{\beta}\right)f'''+Gr\xi^{1-2Z}\left[\theta+Gc\phi\right]\cos\gamma-\left[Ha^2+Zf'\right]f'+\left(\frac{Z+1}{2}\right)ff''=\xi\left[f'\frac{\partial f'}{\partial\xi}-f''\frac{\partial f}{\partial\xi}\right], \tag{9}$$

$$\left[1+\frac{4}{3}N_r\right]\theta''+PrN_b\theta'\phi'+PrN_t\left(\theta'\right)^2+D_u\phi''+\left(\frac{Z+1}{2}\right)Prf\theta'=Pr\xi\left[f'\frac{\partial\theta}{\partial\xi}-\theta'\frac{\partial f}{\partial\xi}\right], \tag{10}$$

$$\phi''+Sr\theta''+Le\left(\frac{Z+1}{2}\right)f\phi'+\frac{N_t}{N_b}\theta''=Le\xi\left[f'\frac{\partial\phi}{\partial\xi}-\phi'\frac{\partial f}{\partial\xi}\right], \tag{11}$$

Subject to;

$$\begin{aligned} &f=-\xi\left(\frac{2}{Z+1}\right)\frac{\partial(\eta,\xi)}{\partial\xi},\ f'=1,\ \xi^{\frac{Z-1}{2}}\theta'(\eta,\xi)=-Bi\left[1-\theta(\eta,\xi)\right],\\ &\phi(\eta,\xi)=1,\quad at\quad \eta=0,\\ &f'(\eta,\xi)=\frac{a}{b}=Q,\quad \theta(\eta,\xi)=0,\quad \phi=0,\qquad at\quad \eta=\infty. \end{aligned} \tag{12}$$

All the relevant parameters are defined in the nomenclature section. The engineering physical quantities of interest are;

$$C_f=\frac{\tau_w}{0.5\rho U_w^2},\quad Nu_x=\frac{xq_w}{\kappa_f(T_w-T_\infty)},\quad Sh_x=\frac{xq_m}{D_b(C_w-C_\infty)}, \tag{13}$$

with surface heat flux and shear stress given by q_w and τ_w respectively

$$\tau_w=\rho\sqrt{a^3\nu}g(\eta),\quad q_w=-\kappa\frac{\partial T}{\partial y}\bigg|_{y=0}-q_r,\quad q_m=-D_b\frac{\partial C}{\partial y}\bigg|_{y=0}. \tag{14}$$

In non-dimensional form, (13) using Eq. (6)–(8) and (14) becomes

$$\begin{aligned} &\frac{1}{2}Re_x^{\frac{1}{2}}C_f=\left(1+\frac{1}{\beta}\right)f''(0,\zeta),\quad Re_x^{-\frac{1}{2}}Nu_x=-\left(1+\frac{4}{3}Nr\right)\theta'(0,\zeta),\\ &Re_x^{-\frac{1}{2}}Sh_x=-\phi'(0,\zeta), \end{aligned} \tag{15}$$

where $Re_x=\frac{U_\infty x}{\nu}$.

3. Numerical method

Different problems involving ordinary differential equations have been solved using spectral collocation technique (SCM). SCM is used, for instance, by Akolade et al. [56] to research the effect of thermo-physical features on squeezed flow. Refs. [57–59] are some references for other works on the considered technique in addressing different physical flow problems. In order to offer a solution for PDEs in Eqs. (9)–(12), the spectral collocation method (SCM) is transformed into the bivariate spectral collocation method (BSCM). In this section, we introduce a modification of the spectral collocation method known as the bivariate spectral collocation method (BSCM) to solve the partial differential equations (PDEs) described by Eqs. (9)–(12).

In the present approach (BSCM), the problem domains $\xi=[0,L_\xi]$ and $\eta=[0,L_\eta]$, where L_ξ is the finite value of dimensionless variable and L_η represent the truncated boundary layer edge. ξ and η are converted to Chebyshev domain $\tau\in[-1,1]$ and $\zeta\in[-1,1]$ using the respective transformation

$$\eta=\frac{L_\eta(\tau+1)}{2}\quad\text{and}\quad\xi=\frac{L_\zeta(\xi+1)}{2}. \tag{16}$$

The partial derivative approximation for functions $f(\tau,\xi)$, $\theta(\tau,\xi)$ and $\phi(\tau,\xi)$ at the Chebyshev–Gauss–Lobatto collocation points $\tau_i=\left\{\cos\left(\frac{\pi i}{N_\tau}\right)\right\}_{i=0}^{N_\tau}$ and $\zeta_j=\left\{\cos\left(\frac{\pi j}{N_\zeta}\right)\right\}_{j=0}^{N_\zeta}$ are given in the form of

differentiation matrices **D** and **d** below (see Uddin et al. [60]).

$$\frac{\partial^{(n)}(f,\theta,\phi)}{\partial\xi^{(n)}} \approx \frac{2}{L_\xi}\sum_{l=0}^{N_\zeta} D_{j,l}^{(n)}(f,\theta,\phi)(i,l) = \mathbf{d}^{(n)}(\bar{f},\bar{\theta},\bar{\phi}),$$
$$\frac{\partial^{(n)}(f,\theta,\phi)}{\partial\eta^{(n)}} \approx \frac{2}{L_\eta}\sum_{k=0}^{N_\tau} D_{i,k}^{(n)}(f,\theta,\phi)(k,j) = \mathbf{D}^{(n)}(\bar{f},\bar{\theta},\bar{\phi}), \tag{17}$$
$$\frac{\partial^2 f}{\partial\xi\partial\eta} \approx \frac{2}{L_\xi}\sum_{l=0}^{N_\xi} d_{j,l}\left(\frac{2}{L_\eta}\sum_{k=0}^{N_\tau} D_{i,k} f(k,l)\right) = \mathbf{d}(\mathbf{D}\bar{f}),$$

with n the order of the differential equations and entries of matrices **D** and **d** as (see, [60,61]).

$$d_{jl} = \frac{c_j}{c_l}\frac{(-1)^{j+l}}{\zeta_j-\zeta_l}, j\neq l, j,l = 0,1,\ldots,N_\zeta,$$
$$d_{ll} = -\frac{\zeta_l}{2(1-\zeta_l^2)}, l = 1,2,\ldots,N_\zeta-1,$$
$$d_{00} = -\frac{2N_\zeta^2+1}{6} = -d_{N_\zeta N_\zeta},$$
and
$$D_{ik} = \frac{c_i}{c_k}\frac{(-1)^{i+k}}{\tau_i-\tau_k}, i\neq k, i,k = 0,1,\ldots,N_\tau, \tag{18}$$
$$D_{kk} = -\frac{\tau_k}{2(1-\tau_k^2)}, k = 1,2,\ldots,N_\tau-1,$$
$$D_{00} = -\frac{2N_\tau^2+1}{6} = -D_{N_\tau N_\tau},$$

with

$$c_k = \begin{cases} 2, & k = 0, N_\tau \\ 1, & -1\leq k\leq N_\tau-1, \end{cases} \text{ and } c_l = \begin{cases} 2, & l = 0, N_\zeta \\ 1, & -1\leq l\leq N_\zeta-1, \end{cases} \tag{19}$$

where

$$\bar{f} = [f(0,0), f(0,1), f(1,0), f(1,1), \ldots, f(N_\tau,N_\zeta)]^T,$$
$$\bar{\theta} = [\theta(0,0), \theta(0,1), \theta(1,0), \theta(1,1), \ldots \theta(N_\tau,N_\zeta)]^T, \tag{20}$$
$$\bar{\phi} = [\phi(0,0), \phi(0,1), \phi(1,0), \phi(1,1), \ldots \phi(N_\tau,N_\zeta)]^T,$$

To obtain solution for Eq. (9) to (12), the following discretized equations are calculated at the grid points $\tau_i(i = 0,1,2,\ldots,N_\chi)$, and $\zeta_j(j = 0,1,2,\ldots,N_\zeta)$, taking into account Eqs. (16)–(20). As such the reduced governing PDEs are discretized as follow:

$$\beta_V\mathbf{D}^3\bar{f} + Gr\zeta_j^{1-2Z}\left[\bar{\theta}+Gc\bar{\phi}\right]\cos\gamma - \left[Ha^2+Z\mathbf{D}\bar{f}\right]\bar{f} + \beta_M\bar{f}\mathbf{D}^2\bar{f} = \zeta_j\left[\mathbf{D}\bar{f}\mathbf{d}(\mathbf{D}\bar{f}) - \mathbf{D}^2\bar{f}\mathbf{d}\bar{f}\right], \tag{21}$$

$$\left[1+\frac{4}{3}N_r\right]\mathbf{D}^2\bar{\theta} + PrN_b\mathbf{D}\bar{\theta}\mathbf{D}\bar{\phi} + PrN_t\mathbf{D}\bar{\theta}\mathbf{D}\bar{\theta} + D_u\mathbf{D}^2\bar{\phi} + \beta_M Pr\bar{f}\mathbf{D}\bar{\theta} = Pr\zeta_j\left[\mathbf{D}\bar{f}\mathbf{d}\bar{\theta} - \mathbf{D}\bar{\theta}\mathbf{d}\bar{f}\right], \tag{22}$$

$$\mathbf{D}^2\bar{\phi} + Sr\mathbf{D}^2\bar{\theta} + Le\beta_M\bar{f}\ \mathbf{D}\bar{\phi} + \frac{N_t}{N_b}\mathbf{D}^2\bar{\theta} = Le\zeta_j\left[\mathbf{D}\bar{f}\mathbf{d}\bar{\phi} - \mathbf{D}\bar{\phi}\ \mathbf{d}\bar{f}\right], \tag{23}$$

where $\beta_V = \left(1+\frac{1}{\beta}\right)$, $\beta_M = \left(\frac{Z+1}{2}\right)$, and $\left(\tau_i(i = 0,2,\ldots,N_\tau),\zeta_j(j = 0,2,\ldots,N_\zeta)\right)$, $\left(\tau_i(i = 1,2,\ldots,N_\tau-2),\zeta_j(j = 0,2,\ldots,N_\zeta)\right)$ and $\left(\tau_i(i = 1,2,\ldots,N_\tau-1),\zeta_j(j = 0,2,\ldots,N_\zeta)\right)$ respectively. Subject to the discretized boundary conditions:

$$\frac{2}{L_\eta}\sum_{k=0}^{N_\tau} D_{N_\tau,k} f(k,j) = 0, \quad f(N_\tau,j) = -\beta_M\frac{2}{L_\eta}\sum_{l=0}^{N_\zeta} d_{N_\zeta,l} f(l,j),$$
$$\frac{2}{L_\eta}\sum_{k=0}^{N_\tau} D_{N_\tau,k}\theta(k,j) - Bi\theta(N_\tau,j) = -Bi, \quad \phi(N_\tau,j) = 1,$$
for $j = 0,1,2,\ldots,N_\zeta$.
$$\frac{2}{L_\eta}\sum_{k=0}^{N_\tau} D_{0,k} f(k,j) = Q, \quad \theta(0,j) = 0, \quad \phi(0,j) = 0 \text{ for } j = 0,1,2,\ldots,N_\zeta. \tag{24}$$

Eqs. (21)–(24) form a system of nonlinear algebraic equations with $3(N_\eta+1)\times(N_\zeta+1)$. These unknowns are obtained using Newton method by implementing **FindRoot** in mathematical symbolic package **MATHEMATICA**.

The numerical scheme exhibits rapid convergence with increasing order of approximations for both N_ζ and N_τ, as evident in Table 1. Specifically, at $N_\zeta = 10$, there is a tolerance difference of up to 10^{-6} observed between $N_\tau = 40$ and $N_\tau = 50$ for the engineering physical quantities. Similarly, for $N_\tau = 50$, a tolerance difference of up to 10^{-4} is observed between $N_\tau = 9$ and $N_\tau = 10$ for the skin friction and Nusselt number. It can be adjudged that for $N_\zeta = 10$ and $N_\tau = 50$, convergence and accuracy of the numerical solution is assured. The residual error which further affirms the stability and convergence of the scheme is depicted in Fig. 2.

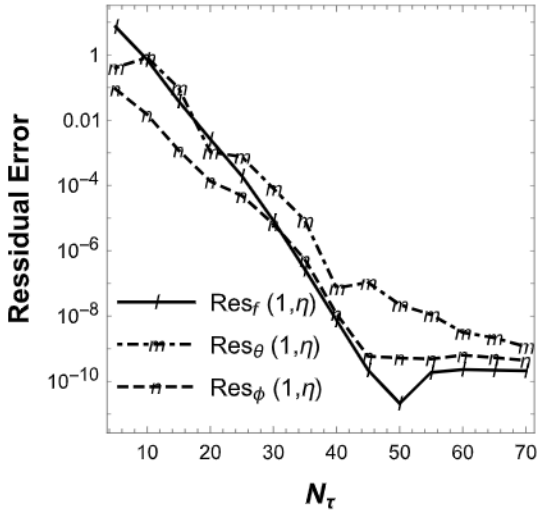

Fig. 2. Residual error norm representing the convergence of the model as N_τ increases and $N_\zeta = 10$, $Ha = 0.5$, $\beta = 0.5$, $Gr = 1.0$, $Gc = 1$, $Pr = 1.0$, $Sc = 2.0$, $N_t = 0.1$, $N_b = 0.4$, $Sr = 0.4$, $Nr = 0.1$, $Du = 0.1$, $Z = 0.5$, $\gamma = \pi/4$, $Q = 0.01$, $Bi = 1$.

4. Results and discussion

4.1. Results of distribution profiles $f'(\zeta,\eta)$, $\theta(\zeta,\eta)$, and $\phi(\zeta,\eta)$

This article numerically investigates the dynamics of accelerating and decelerating flow of hydromagnetic flow of a Casson fluid over a slanted vertical plate with the influence of Soret and Dufour effects and thermal radiation. By introducing the non-similar transformation approach, the system of equations governing the flow with boundary conditions are highly non-linear in nature and complex to obtain any exact solutions. To accomplish the research objective, the present study employs the Spectral collocation method for handling these non-linear differential equations in Mathematica and results are performed

Table 1
Convergence solution of BSCM for different approximation's orders when: $Ha = 0.5$, $\beta = 0.5$, $Gr = 1.0$, $Gc = 1$, $Pr = 1.0$, $Sc = 2.0$, $N_t = 0.1$, $N_b = 0.4$, $Sr = 0.4$, $Nr = 0.1$, $Du = 0.1$, $Z = 0.5$, $\gamma = \pi/4$, $Q = 0.01$, $Bi = 1$.

Order $N_\zeta = 10$	$\frac{1}{2}Re_x^{\frac{1}{2}}C_f$	$Re_x^{-\frac{1}{2}}Nu_x$	$Re_x^{-\frac{1}{2}}Sh_x$	Order $N_\tau = 50$	$\frac{1}{2}Re_x^{\frac{1}{2}}C_f$	$Re_x^{-\frac{1}{2}}Nu_x$	$Re_x^{-\frac{1}{2}}Sh_x$
$N_\tau = 10$	−0.48707	0.316403	0.846396	$N_\zeta = 02$	−1.45823	0.330145	0.51957
$N_\tau = 20$	−1.47206	0.315825	0.776300	$N_\zeta = 04$	−1.46951	0.312062	0.657011
$N_\tau = 30$	−1.46714	0.315874	0.775476	$N_\zeta = 06$	−1.46809	0.314348	0.725461
$N_\tau = 40$	−1.46713	0.315874	0.775471	$N_\zeta = 07$	−1.46789	0.315821	0.742431
$N_\tau = 50$	−1.46713	0.315874	0.775471	$N_\zeta = 08$	−1.46741	0.315423	0.757388
$N_\tau = 60$	−1.46712	0.315874	0.775471	$N_\zeta = 09$	−1.46721	0.315611	0.767221
$N_\tau = 70$	−1.46712	0.315874	0.775471	$N_\zeta = 10$	−1.46713	0.315874	0.775471

for both accelerating and decelerating flow situations respectively. The uniqueness of this current investigation is concerned with the immediate emerging engineering applications as visualized in many aerodynamic and fluid mechanics problems in air flow around an aircraft and brunet of a moving vehicle. During the course of the numerical computations, relevant influence of pertinent flow parameters on flow dynamics are highlighted to incorporate the influences of the Casson parameter, thermal radiation parameter, magnetic parameter, as well as Soret and Dufour parameters. Figs. 3(a, b, c) Illustrate the impression of the Casson fluid flow parameter (β) on the velocity curve, temperature distribution, and fluid concentration for both accelerating and decelerating flow situations in the existence of thermal radiation (N_r). From Fig. 3(a), increment in (β) is clearly observed to attenuate the velocity profile for both accelerating and decelerating flow situation. This is owing to the physical fact that the fluid yield stress demonstrates an inverse relationship with (β). Hence, enhancing the values of (β) weakens the fluid yield stress leading to decrease in fluid velocity as observed for both accelerating and decelerating flow situations. It is however interesting to mention that higher values of (β) significantly augment fluid concentration and temperature distribution for accelerating flow situation whereas the opposite phenomenon is observed for decelerating flow situation. In a situation where the flow is accelerating, enhancing (β) advances the chemical specie and reduces the thermal boundary layer resulting in the accumulation of heat and consequently leading to an increase in the distribution of fluid temperature as observed in Figs. 3(b) and (c) respectively. Figs. 4(a) and (b) illustrate the impression of magnetic parameter(Ha) and inclination angle (γ) on velocity curve for both accelerating and decelerating flow situation. Fig. 4(a) shows that in the occurrence of thermal diffusion and thermal radiation, higher values of Ha enhances the fluid viscosity profile causing a decrease in velocity profile. This is evident for both accelerating and decelerating flow situation. Increase in inclination angle on the other hand weakens the buoyancy current leading to decrease in velocity curve (Fig. 4(b)).

Influence of Biot number (Bi) on temperature and concentration profile is illustrated in Fig. 5(a) and (b) for both decelerating and accelerating flow situations. Details from the figure demonstrate that higher fluid concentration and temperature could be achieved by growing the convective current parameter. Thus, the thermal boundary layer about the plate could be reduced by increasing the Bi thereby increasing the concentration profile and subsequently the temperature distribution. The role Dufour parameter on the fluid temperature for accelerating and decelerating flow is represented in Fig. 6(a). It can be justified that the fluid temperature exhibits a direct proportionality with the Dufour parameter (D_u) for the two cases under consideration. This is associated with the fact that growth in the D_u increases the concentration gradient, resulting in high mass diffusion and in turn increasing the temperature distribution. The influence of R on fluid temperature in both assisting and opposing flows is demonstrated in Fig. 6(b). The figure suggests that R augment leads to an upsurge in thermal boundary layer thickness. Furthermore, it can be inferred that the temperature rise is a result of the absorption of radiative heat emitted by the heated inclined plate. This phenomenon amplifies the buoyancy force due to the increase in fluid temperature, consequently encouraging the formation of flow within the boundary layer. Fig. 7 describes the impression of the Brownian motion parameter (N_b) on the temperature and concentration for accelerating and decelerating flow. Observation from the Figures revealed that the nanofluid temperature enhanced with Nb growth whereas decreases the rate of nanoparticle concentration. In a physical context, the inclined boundary layer experiences warming due to heightened Brownian motion, causing the transfer of nanoparticles from the extending plate to the stationary liquid. As a result, the nanoparticle absorption rate decreases.

Fig. 8 shows the importance of the thermophoresis parameter (N_t) on the temperature distribution and concentration profile for accelerating and deceleration flow. It can be understood from the Figure that the fluid temperature and nanoparticle diffusion increase with N_t augment due to the fact that thermophoresis cause the nanoparticle in a high energy level or hot region to compel the nanoparticle toward the cold region. Due to this effect, the heat transfer rate is increased by transporting the hot nanoparticle from the hot region to the cold region. Fig. 9 shows the role Soret number on the concentration profile for accelerating and decelerating flow. It can be inferred from the Figure that the rate of particle diffusion rise as the Soret number intensifies. Soret number is the fraction of temperature variation (between the plate and the ambient fluid) to concentration, hence higher Soret number corresponds to higher temperature variation and precipitous gradient.

4.2. Results of engineering quantities of interest

Table 2 demonstrates the variation active flow parameters on the skin friction Sherwood number and Nusselt number for accelerating and decelerating flow. The table suggests that for accelerating and decelerating flow scenarios, the shear stress and mass transfer increases with growth in β, N_t, N_b, N_r, Du, Bi and S_r whereas decreases with Ha. This phenomenon is expected because, the surge in enhances the fluid transport and particle diffusion in the boundary layer which give rise to the plate shear stress and mass transfer. Furthermore, the radiative heat flux decreases the fluid transport near the plate leading in the increases in the shear stress. The Sherwood number significantly increase with N_b and Du increase but decreases with β, N_t, N_r, Bi, Ha and S_r. The thermal boundary layer thickness enhanced as a result of the increase in the Brownian motion parameter, impacting a significant volume of the fluid. Moreover, higher thermophoresis force reduces the Sherwood number owning to the fact that the thermal boundary layer thickens as a result of increased diffusion penetration into the fluid particles. The magnetic parameter retards the fluid flow there by reducing rate of particle diffusion near the plate edge and within the surrounding free stream. In addition, the radiative heat flux induces more heat energy into the fluid resulting in substantial increase in the velocity profile and in turn enhances the rate particle diffusion on the plate surface.

It is seen that increase in β improves the heat transfer for both accelerating and decelerating flow situations. A close examination of the Table shows that in the incidence of N_r and S_r as well as D_u effects, the influence of β is less pronounced on heat transfer near the boundary

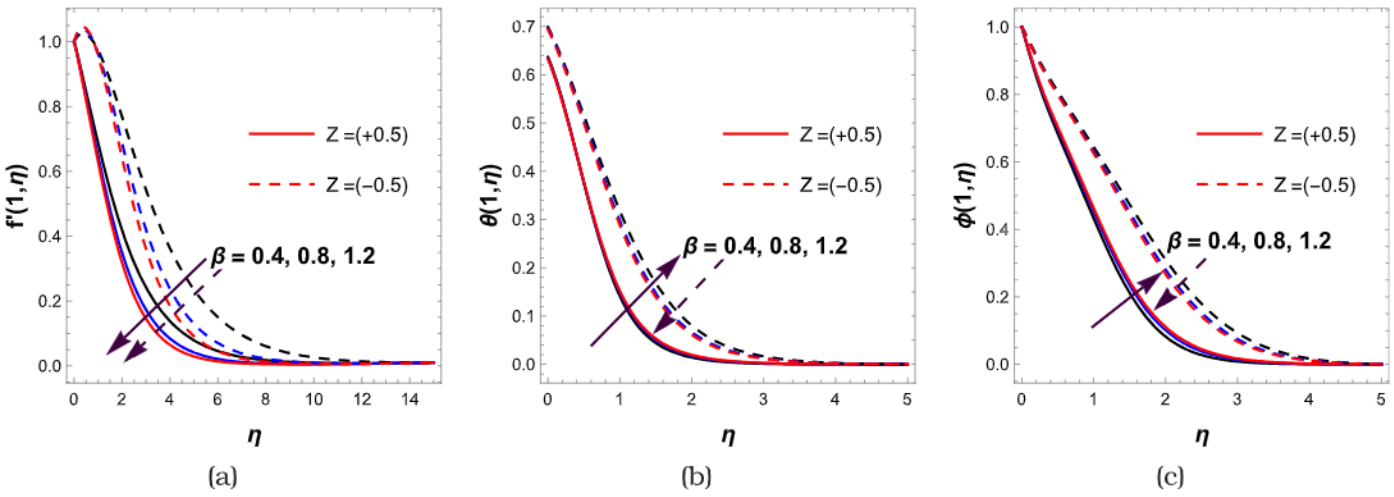

Fig. 3. Importance of β variation on (a) velocity profile (b) temperature distribution and (c) concentration profile.

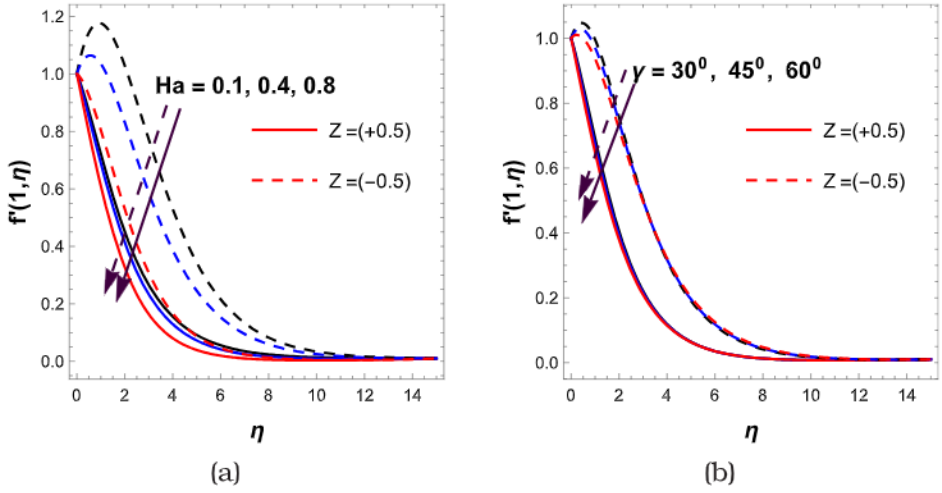

Fig. 4. Velocity profiles for various(a) magnetic parameter (b) inclination parameter.

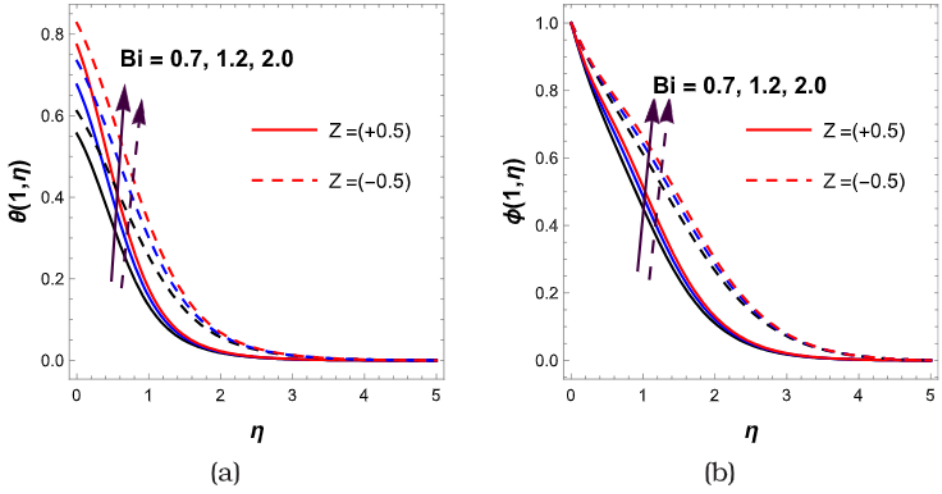

Fig. 5. Importance of *Bi* variation on (a) temperature distribution (b) concentration profile.

plate resulting in negligible variation on temperature field about the plate whereas the influence becomes noticeable far away from the plate. Additionally, it is noted that an increase in the *Bi* considerably amplifies the heat transfer for both accelerating and decelerating flow situations. This phenomenon is attributed to the physical reality that an increase in the Biot number enhances heat accumulation in the system leading to increase in temperature distribution. In addition, the Table also suggest that increase in Soret number and thermal radiation

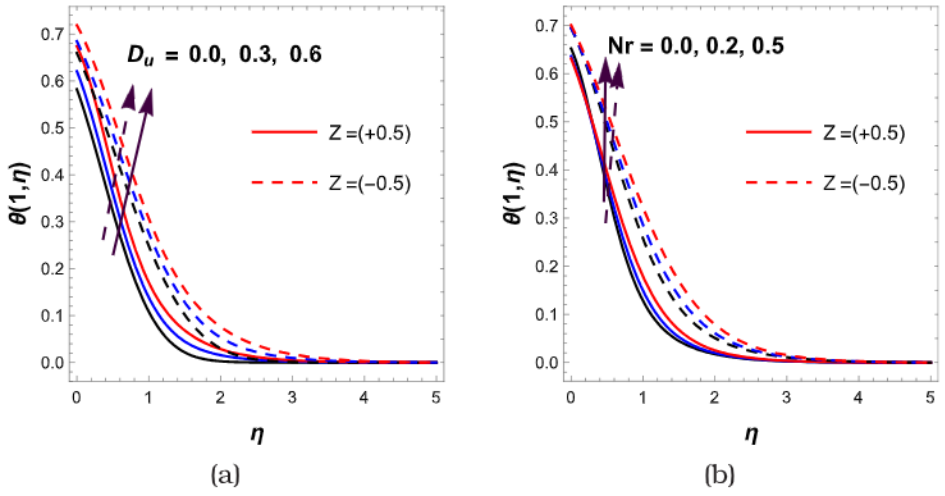

Fig. 6. Temperature curve for various (a) Dufour parameter (b) thermal radiation parameter.

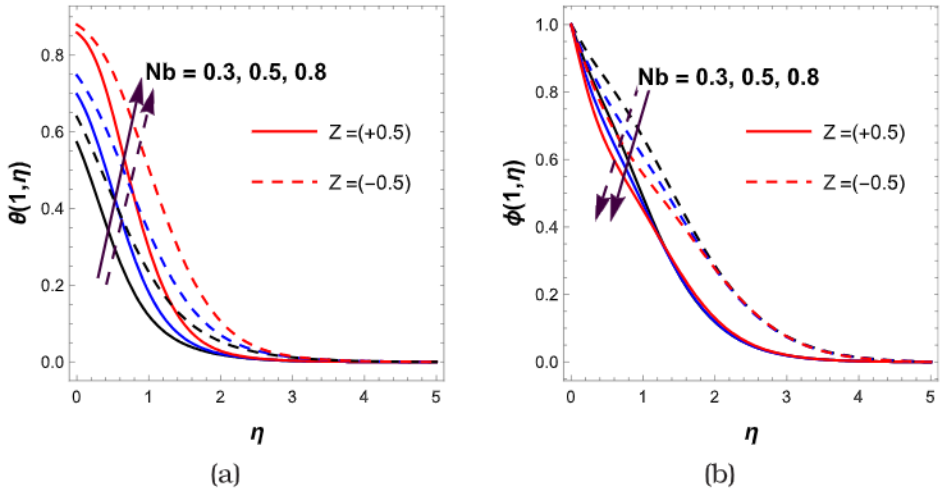

Fig. 7. Importance of N_b on (a) temperature distribution (b) concentration profile.

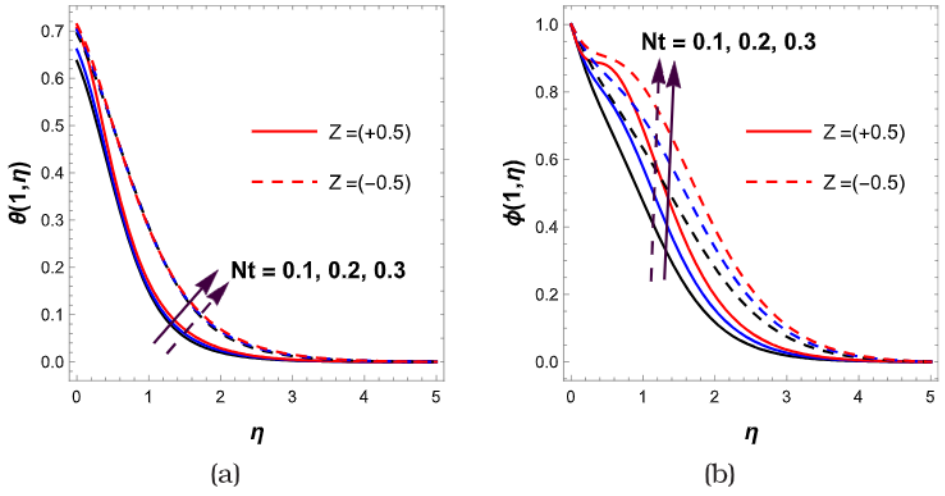

Fig. 8. Importance of N_t on (a) temperature distribution (b) concentration profile.

Table 2
Computational results of engineering quantities of interest with variation of model parameters (β, γ, Ha,) when: $Ha = 0.5$, $\beta = 0.5$, $Gr = 1.0$, $Gc = 1.0$, $Pr = 6.8$, $Sc = 2.0$, $N_t = 0.1$, $N_b = 0.4$, $Sr = 0.4$, $Nr = 0.3$, $Du = 0.4$, $\gamma = \pi/3$, $Q = 0.01$, $Bi = 1$.

		$Z > 0$ (accelerating flow), $Z = 0.5$			$Z < 0$ (decelerating flow), $Z = -0.5$		
		$\frac{1}{2}Re_x^{\frac{1}{2}}C_f$	$Re_x^{-\frac{1}{2}}Nu_x$	$Re_x^{-\frac{1}{2}}Sh_x$	$\frac{1}{2}Re_x^{\frac{1}{2}}C_f$	$Re_x^{-\frac{1}{2}}Nu_x$	$Re_x^{-\frac{1}{2}}Sh_x$
β	0.3	−1.294620	0.508350	0.735862	0.316409	0.419584	0.42027
	0.5	−1.00787	0.50968	0.714931	0.324829	0.421331	0.415797
	1.0	−0.753475	0.511507	0.689597	0.321845	0.424238	0.406996
Ha	0.1	−0.760606	0.509651	0.739757	1.106200	0.423332	0.497003
	0.3	−0.847304	0.509661	0.731028	0.804141	0.422349	0.467972
	0.7	−1.22436	0.509697	0.693328	−0.161800	0.421800	0.354304
B_i	0.5	−1.06053	0.362473	0.749317	0.259504	0.327308	0.431664
	1.0	−1.00787	0.50968	0.714931	0.324829	0.421331	0.415797
	1.5	−0.979414	0.590575	0.695446	0.358574	0.457492	0.412784
N_t	0.1	−1.00787	0.50968	0.714931	0.324829	0.421331	0.415797
	0.3	−0.925167	0.46131	0.704822	0.395509	0.399119	0.364469
	0.5	−0.822831	0.324737	1.08299	0.484632	0.34576	0.444285
N_b	0.2	−1.02736	0.680777	0.450532	0.304711	0.57572	0.196739
	0.5	−0.99004	0.430958	0.779516	0.343015	0.353807	0.467133
	0.7	−0.949841	0.285959	0.866215	0.383614	0.232114	0.534593
Sr	0.1	−1.02148	0.488022	0.758197	0.313623	0.399808	0.453672
	0.3	−1.01231	0.502083	0.730709	0.321159	0.413706	0.429741
	0.5	−1.00355	0.517693	0.697588	0.328415	0.429465	0.400298
N_r	0.0	−1.01239	0.351828	0.744433	0.316588	0.302173	0.42533
	0.2	−1.00991	0.458786	0.72124	0.321848	0.383014	0.417403
	0.5	−1.00314	0.607609	0.707559	0.330925	0.494811	0.414755
B_i	0.5	−1.06053	0.362473	0.749317	0.259504	0.327308	0.431664
	0.7	−1.03493	0.434049	0.732703	0.291576	0.377205	0.422347
	0.9	−1.01575	0.487605	0.720152	0.31524	0.409449	0.417336
D_u	0.0	−1.03302	0.575615	0.666809	0.304893	0.466753	0.386335
	0.2	−1.02104	0.545184	0.688605	0.314338	0.445842	0.399647
	0.5	−1.00070	0.489397	0.730398	0.330589	0.407284	0.42531

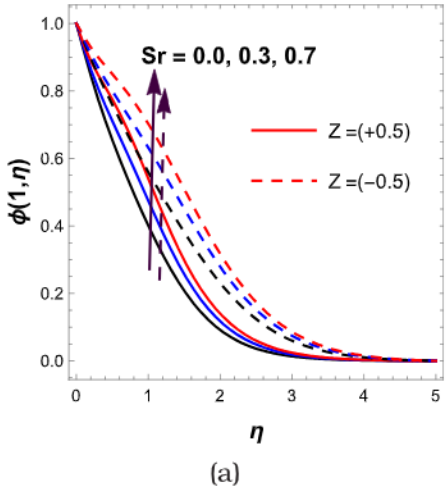

Fig. 9. Concentration profile for various §$_r$.

contributes to surge in rate of heat transfer whereas the contrast is observed with Dufour.

5. Conclusions

This study explored the dynamics of accelerating and decelerating flows near an inclined plate. The solution to the dimensionless equations describing the fluid features were achieved through bivariate spectral collocation method (BSCM) in mathematical symbolic package MATHEMATICA. The effect of the active parameters affecting the flow feature has been presented through line graphs and tables. It is noted that the effect of the convective boundary condition at the wall for variation in the Brownian motion parameter is approximately 2.298%–8.333% increment between the accelerating and decelerating flows. The results show that:

- Increasing the Biot number by 40% and 28.6% respectively, the skin friction of the decelerating flow increase by 12.359% and 8.115%. While the skin friction of the accelerating flow increase by 2.413% and 1.853%. The Biot parameter positively impacts the velocity and temperature profiles of both decelerating and accelerating flows.
- The temperature profile shows a 9.375% increase in the accelerating flow compared to the decelerating flow at the wall with variation in β. An increase in the fluid parameter β has an opposing effect on the temperature and concentration profiles of both flows.
- The effects of flow parameters on decelerating and accelerating flows are not completely opposite.
- The inclined boundary layer warmth up due to the increase in the Brownian motion which transports nanoparticles from the extending plate to the motionless liquid and consequently lessens the rate of absorption of nanoparticles.
- The fluid temperature and nanoparticle diffusion increase with Nt augment because, Nt causes the nanoparticle in a high energy level or hot region to compel the nanoparticle toward the cold region.
- Increasing the Hartmann number by 200% and 133.33% respectively, the Sherwood number of the accelerating flow decrease by 1.179% and 5.157%. While the Sherwood number of the decelerating flow decrease by 5.841% and 24.289%. Increasing the

magnitude of the Hartmann number, downsize the skin friction and Nusselt number in the decelerating flow.

CRediT authorship contribution statement

Mojeed T. Akolade: Formal analysis and methodology. **Gabriel Samaila:** Conceptualization and discussion of results. **Micheal Oni:** Methodology and model validation. **Abdulhakeem Yusuf:** Validation and results discussion. **Peter Bukar Malgwi:** Project administration and literature analysis. **Taiwo S. Yusuf:** Software and result verification. **Yusuf O. Tijani:** Supervision and code validation.

Declaration of competing interest

The authors declare that there is no conflict of interest.

Data availability

Data will be made available on request.

Acknowledgment

The authors express gratitude to the anonymous reviewers and congratulate the seven founding members of the "Computational Mechanics and Mathematical Modelling Research Group (CMMMRG)" on its first collaborative publication. To strengthen the research group, the group is open for collaboration and research activities.

References

[1] L.J. Sundstrom, M.J. Cervantes, Laminar similarities between accelerating and decelerating turbulent flows, Int. J. Heat Fluid Flow 71 (2018) 13–26.
[2] L.J. Sundstrom, M.J. Cervantes, The self-similarity of wall-bounded temporally accelerating turbulent flows, J. Turbul. 19 (1) (2018) 49–60.
[3] M. Seddighi, S. He, A.E. Vardy, P. Orlandi, Direct numerical simulation of an accelerating channel flow, flow, turbulence and combustion, 92, 2014, pp. 473–502.
[4] B. Guerrero, M.F. Lambert, R.C. Chin, Transient behaviour of decelerating turbulent pipe flows, J. Fluid Mech. 962 (2023) A44.
[5] S.Y. Jung, K. Kim, Transient behaviors of wall turbulence in temporally accelerating channel flows, Int. J. Heat Fluid Flow 67 (2017) 13–26.
[6] E.B. Shuy, Wall shear stress in accelerating and decelerating turbulent pipe flows, J. Hydraul. Res. 34 (2) (1996) 173–183.
[7] B.K. Jha, L.A. Azeez, M.O. Oni, Unsteady hydromagnetic-free convection flow with suction/injection, J. Taibah Univ. Sci. 13 (1) (2019) 136–145.
[8] E.M. Sparrow, H. Quack, C.J. Boerner, Local non-similarity boundary layer solutions, Am. Inst. Aeronaut. Astronat. J. 8 (11) (1970) 1936–1942.
[9] Pantokratoras A., A common error made in investigation of boundary layer flows, Appl. Math. Model. 33 (1) (2009) 413–422.
[10] Pantokratoras A., Four usual errors made in investigation of boundary layer flows, Powder Technol. 353 (2019) 505–508.
[11] X. Chen, Y. Ye, X. Zhang, L. Zheng, Lie-group similarity solution and analysis for fractional viscoelastic MHD fluid over a stretching sheet, Comput. Math. Appl. 75 (8) (2018) 3002–3011.
[12] H.A. Ogunseye, S.O. Salawu, S.D. Oloniiju, M.T. Akolade, Y.O. Tijani, R. Mustapha, P. Sibanda, MHD Powell–eyring nanofluid motion with convective surface condition and dufour–soret impact past a vertical plate: Lie group analysis, Partial Differential Equations in Applied Mathematics 6 (2022) 100459.
[13] D. Pal, N. Roy, Lie group transformation on MHD double-diffusion convection of a Casson nanofluid over a vertical stretching/shrinking surface with thermal radiation and chemical reaction, Int. J. Appl. Comput. Math. 4 (2018) 1–23.
[14] G. Nath, A. Devi, Similarity solution using group theoretic method for unsteady flow behind shock wave in a self-gravitating dusty gas, Int. J. Non-Linear Mech. 148 (2023) 104254.
[15] M.O. Lawal, S.O. Ajadi, Local nonsimilarity solution of Casson fluid flow along a stretching surface in the presence of viscous dissipation, variable viscosity and thermal conductivity, J. Nigerian Math. Soc. 40 (3) (2021) 269–300.
[16] F.M. White, Viscous Fluid Flow, third ed., McGraw-Hill, New York, 2006, pp. 146–147.
[17] A. Bisht, R. Sharma, Non-similar solution of Casson nanofluid with variable viscosity and variable thermal conductivity, Internat. J. Numer. Methods Heat Fluid Flow 22 (8) (2020) 3919–3938.
[18] R. Khademi, A. Razminia, V.I. Shiryaev, Conjugate-mixed convection of nanofluid flow over an inclined flat plate in porous media, Appl. Math. Comput. 366 (2020) 124761.
[19] A. Kaya, Effects of conjugate heat transfer on steady MHD mixed convective heat transfer flow over a thin vertical plate embedded in a porous medium with high porosity, Math. Probl. Eng. 2012 (2012).
[20] K.A. Yih, Viscous and joule heating effects on non-Darcy MHD natural convection flow over a permeable sphere in porous media with internal heat generation, Int. Commun. Heat Mass Transf. 27 (4) (2000) 591–600.
[21] Y.O. Tijani, A.T. Adeosun, H.A. Ogunseye, H. Niranjan, Magnetic dipole dynamics on Reiner–Philippoff boundary layer flow, Numer. Heat Transf. A: Applications (2023) 1–15.
[22] Y.O. Tijani, S.D. Oloniiju, K.B. Kasali, M.T. Akolade, Nonsimilar solution of a boundary layer flow of a Reiner–Philippoff fluid with nonlinear thermal convection, Heat Transf. 51 (6) (2022) 5659–5678.
[23] Y.O. Tijani, S.D. Oloniiju, O. Otegbeye, A.R. Babalola, Magnetic feature and regression analysis of Reiner-Philippoff boundary layer flow, Numer. Heat Transfer B (2023) 1–19.
[24] I. Mustafa, S. Shahbaz, A. Ghaffari, T. Muhammad, Non-similar solution for a power-law fluid flow over a moving wedge, Alex. Eng. J. 75 (2023) 287–296.
[25] J. Cui, R. Razzaq, U. Farooq, W.A. Khan, F.B. Farooq, T. Muhammad, Impact of non-similar modeling for forced convection analysis of nano-fluid flow over stretching sheet with chemical reaction and heat generation, Alex. Eng. J. 61 (6) (2022) 4253–4261.
[26] U. Farooq, M. Safeer, J. Cui, M. Hussain, N. Naheed, Forced convection analysis of williamson-based magnetized hybrid nanofluid flow through a porous medium: Nonsimilar modeling, Numer. Heat Transfer B (2024) 1–17.
[27] N. Gajjela, M. Garvandha, The influence of magnetized couple stress heat, and mass transfer flow in a stretching cylinder with convective boundary condition, cross-diffusion, and chemical reaction, Therm. Sci. Eng. Progress 18 (2020) 100517.
[28] I. Tlili, H. Waqas, A. Almaneea, S.U. Khan, M. Imran, Activation energy and second order slip in bioconvection of Oldroyd-B nanofluid over a stretching cylinder: A proposed mathematical model, Processes 7 (12) (2019) 914.
[29] A. Shojaei, A.J. Amiri, S.S. Ardahaie, K. Hosseinzadeh, D.D. Ganji, Hydrothermal analysis of non-Newtonian second grade fluid flow on radiative stretching cylinder with Soret and Dufour effects, Case Stud. Therm. Eng. 13 (2019) 100384.
[30] M. Jawad, et al., Analytical study of MHD mixed convection flow for Maxwell nanofluid with variable thermal conductivity and Soret and Dufour effects, AIP Adv. 11 (3) (2021) 035215.
[31] M. Ramzan, M. Bilal, J.D. Chung, Soret and Dufour effects on three dimensional upper-convected Maxwell fluid with chemical reaction and non-linear radiative heat flux, Int. J. Chem. React. Eng. 15 (3) (2017) 20160136.
[32] M. Ramzan, F. Yousaf, M. Farooq, J.D. Chung, Mixed convective viscoelastic nanofluid flow past a porous media with soret -dufour effects, Commun. Theor. Phys. 66 (1) (2016) 133.
[33] M. Ramzan, M. Farooq, T. Hayat, A. Alsaedi, J. Cao, MHD stagnation point flow by a permeable stretching cylinder with soret-dufour effects, J. Cent. South Univ. 22 (2) (2015) 707–716.
[34] G.C. Layek, B. Mandal, K. Bhattacharyya, Dufour and soret effects on unsteady heat and mass transfer for powell-eyring fluid flow over an expanding permeable sheet, J. Appl. Comput. Mech. 6 (4) (2020) 985–998.
[35] A.V. Ramudu, K.A. Kumar, V. Sugunamma, N. Sandeep, Impact of Soret and Dufour on MHD Casson fluid flow past a stretching surface with convective–diffusive conditions, J. Therm. Anal. Calorim. (2021).
[36] K.B. Kasali, Y.O. Tijani, M.O. Lawal, Y.T. Soret Lawal, Dufour and radiation effects of a viscoelastic fluid on an exponentially stretching surface using the catteneo–christov heat flux model, Multidiscipline Model. Mater. Struct. (2020).
[37] R.K. Dash, K.N. Mehta, G. Jayaraman, Casson fluid flow in a pipe filled with a homogeneous porous medium, Internat. J. Engrg. Sci. 34 (10) (1996) 1145–1156.
[38] Y.C. Fung, Bio Dynamics Circulation, Springer-Verlag, New York, 1984.
[39] A. Khalid, I. Khan, A. Khan, S. Shafie, Unsteady MHD free convection flow of Casson fluid past over an oscillating vertical plate embedded in a porous medium, Eng. Sci. Technol. Int. J. 18 (3) (2015) 309–317.
[40] S. Oka, An approach to unified theory of the flow behavior of time-independent non-Newtonian suspensions, Japan. J. Appl. Phys. 10 (3) (1971) 287.
[41] K. Bhattacharyya, T. Hayat, A. Alsaedi, Analytic solution for magnetohydrodynamic boundary layer flow of Casson fluid over a stretching/shrinking sheet with wall mass transfer, Chin. Phys. B 22 (2) (2013) 024702.
[42] A.V. Mernone, J.N. Mazumdar, S.K. Lucas, A mathematical study of peristaltic transport of a Casson fluid, Math. Comput. Modelling 35 (7–8) (2002) 895–912.
[43] M. Mustafa, T. Hayat, I. Pop, A. Aziz, Unsteady boundary layer flow of a Casson fluid due to an impulsively started moving flat plate, Heat Transf. 40 (6) (2011) 563–576.
[44] S. Mukhopadhyay, Effects of thermal radiation on Casson fluid flow and heat transfer over an unsteady stretching surface subjected to suction/blowing, Chin. Phys. B 22 (11) (2013) 114702.
[45] S. Pramanik, Casson fluid flow and heat transfer past an exponentially porous stretching surface in presence of thermal radiation, Ain Shams Eng. J. 5 (1) (2014) 205–212.

[46] E.M. Arthur, I.Y. Seini, L.B. Bortteir, Analysis of Casson fluid flow over a vertical porous surface with chemical reaction in the presence of magnetic field, J Appl. Math. Phys. 3 (2015) 713–723.
[47] Talha Anwar, Poom Kumam, Wiboonsak Watthayu, Unsteady mhd natural convection flow of Casson fluid incorporating thermal radiative flux and heat injection/suction mechanism under variable wall conditions, Sci. Rep. 11 (2021) 4275.
[48] J. Singh, A.B. Vishalakshi, U.S. Mahabaleshwar, G. Bognar, MHD Casson fluid flow with Navier's and second order slip due to a perforated stretching or shrinking sheet, PLoS ONE 17 (11) (2022) e0276870.
[49] J. Raza, Thermal radiation and slip effects on magnetohydrodynamic (MHD) stagnation point flow of Casson fluid over a convective stretching sheet, Propul. Power Res. 8 (2019) 138–146.
[50] L.A. Lund, Z. Omar, J. Raza, I. Khan, E.S.M. Sherif, Effects of stefan blowing and slip conditions on unsteady MHD Casson nanofluid flow over an unsteady shrinking sheet: Dual solutions, Symmetry 12 (2020) 487.
[51] U.S. Mahabaleshwar, M.B. Rekha, P.N.V. Kumar, F. Selimefendigi, P.H. Sakanaka, G. Lorenzini, et al., Mass transfer characteristics of MHD Casson fluid flow past stretching/shrinking sheet, J. Eng. Thermophys. 29 (2) (2020) 285–302.
[52] B.C. Sakiadis, Boundary-layer behavior on continuous solid surfaces: I. Boundary-layer equations for two-dimensional and axisymmetric flow, AIChE J. 7 (1961) 26–28.
[53] B.C. Sakiadis, Boundary-layer behavior on continuous solid surfaces: II. The boundary layer on a continuous flat surface, AIChE J. 7 (1961) 221–225.
[54] E.H. Aly, I. Pop, MHD flow and heat transfer near stagnation point over a stretching/shrinking surface with partial slip and viscous dissipation: Hybrid nanofluid versus nanofluid, Powder Technol. 367 (2020) 192–205.
[55] R. Mohamad, M. Ismoen, Local non-similarity solution for MHD mixed convection flow of a nanofluid past a permeable vertical plate in the presence of thermal radiation effects, J. Appl. Comput. Math. 4 (6) (2015) 1–9.
[56] M.T. Akolade, A.T. Adeosun, Olabode. J., Influence of thermophysical features on MHD squeezed flow of dissipative Casson fluid with chemical and radiative effects, J. Appl. Comput. Mech. 7 (4) (2021) 1999–2009.
[57] Y.O. Tijani, M.T. Akolade, H.A. Ogunseye, A.T. Adeosun, O. Farotimi, On the generalized Fick's and Fourier's laws for an unsteady Casson-Williamson fluids over a stretching surface: A spectral approach, J. Nanofluids 12 (1) (2023) 91–103.
[58] T.A. Adeshina, C.U. Joel, Effect of the variable electrical conductivity on the thermal stability of the MHD reactive squeezed fluid flow through a channel by a spectral collocation approach, Partial Differential Equ. Appl. Math. 5 (2022) 100256.
[59] E.O. Fatunmbi, A.T. Adeosun, S.O. Salawu, Entropy analysis of nonlinear radiative Casson nanofluid transport over an electromagnetic actuator with temperature-dependent properties, Partial Differential Equ. Appl. Math. 4 (2021) 100152.
[60] M.J. Uddin, M.N. Kabir, O.Anwar. B'eg, Y. Alginahi, Chebyshev collocation computation of magneto-bioconvection nanofluid flow over a wedge with multiple slips and magnetic induction, Proc. Inst. Mech. Eng. N 232 (4) (2018) 109–122.
[61] S.S. Motsa, On the practical use of the spectral homotopy analysis method and local linearisation method for unsteady boundary-layer flows caused by an impulsively stretching plate, Numer. Algorith. 66 (2014) 865–883.